Available online at www.sciencedirect.com
SCIENCE DIRECT
Catalysis Today 114 (2006) 272–280
CATALYSIS TODAY
www.elsevier.com/locate/cattod

Effect of MCM-41 on the physicochemical properties of Mo and NiMo catalysts and their performance in DBT conversion

Jolanta R. Grzechowiak [a,*], Karolina Mrozińska [a], Aleksandra Masalska [a], Jacek Góralski [b], Jacek Rynkowski [b], Włodzimierz Tylus [c]

[a] *Department of Chemistry and Technology of Fuel, Faculty of Chemistry, Wrocław University of Technology, 7/9 Gdańska Str., 50-344 Wrocław, Poland*
[b] *Institute of General and Ecological Chemistry, Technical University of Łódź, 36 Żwirki Str., 90-924 Łódź, Poland*
[c] *Institute of Inorganic Technology, Faculty of Chemistry, Wrocław University of Technology, Smoluchowskiego Str., 50-353 Wrocław, Poland*

Available online 14 February 2006

Abstract

The influence of mesoporous materials on the properties and HDS activity of Mo and NiMo catalysts was investigated for supports containing 50 wt.% of MCM-41. A series of catalysts was characterized by different techniques (S_{BET}, TPD-NH_3, TPR, SEM, XPS) and tested in dibenzothiophene (DBT) conversion. On the surface of the catalysts containing mesoporous materials, agglomerations of the Mo oxo-species were observed. The presence of MCM-41 in the support visibly weakened the promoting effect of TiO_2 on the reducibility of Mo oxides. The results of DBT HDS showed that the NiMo catalyst supported on MCM-41 was not only less efficient than that supported on Al_2O_3 but also that supported on Al_2O_3–TiO_2. From the distribution of DBT HDS products we can conclude that over catalysts containing MCM-41 the desulphurization of DBT runs mostly via the DDS route.

Keywords: DBT HDS; Al_2O_3–TiO_2; Al_2O_3; MCM-41; NiMo catalysts

1. Introduction

To develop high-performance HDS catalysts it is advisable to focus research on the conversion of DBT and/or DBT derivatives that are known to be the most refractory S-containing compounds. Of the DBT derivatives, some of polyaromatic sulphur compounds show reactivities 50-fold lower as compared to others [1]. The concentration of the most refractory sulphur compounds in straight-run diesel oil and light cycle oil approaches 3000 and 5000 ppm, respectively [2,3].

The modification of the physicochemical properties of the supports is one of the still preferred modes of increasing catalytic activity. The support effects on the activity of hydrotreating catalysts have been reviewed elsewhere [4,5]. The synthesis of mesoporous molecular sieves with high surface area and relatively ordered pore structure offers new possibilities of using these materials as modifiers of the porous support structure. Reddy et al. [6] have applied the CoMo/AlMCM-41 catalyst for upgrading the petroleum residue. They have found that the CoMo/AlMCM-41 catalyst was not as active as the commercial CoMo/Al_2O_3, and they have stated that the pore size of MCM-41 is not large enough to convert such molecules as those of the asphalthenes present in this feed. Cheng et al. [7] have investigated molybdenum catalysts on extruded Al_2O_3-AlMCM-41, using two model reactions: with a small reactant, thiophene, and a large reactant, nickel tetraphenylporphyrin (Ni-TPP). Investigating the structure of Mo oxide and Mo sulphide species inside the channels of AlMCM-41 and in the mesopore system of Al_2O_3, they have found that the catalysts supported on mesoporous molecular sieves can be expected to offer a high activity for deep hydrotreating of the light fraction of petroleum oil. According to Ramírez et al. [8], the activity of the catalyst

* Corresponding author. Tel.: +487 1320 6207; fax: +487 1322 1580.
E-mail address: Jolanta.Grzechowiak@nw.pwr.wroc.pl (J.R. Grzechowiak).

0920-5861/$ – see front matter © 2006 Elsevier B.V. All rights reserved.
doi:10.1016/j.cattod.2006.01.004

containing AlMCM-41 (Al_2O_3-AlMCM-41) is higher in the DBT HDS reaction than the activity of the catalyst supported on pure alumina.

The aim of our study was to compare the physicochemical properties and activity of Mo and NiMo HDS catalysts based on SiMCM-41 alone and of the same catalysts based on supports where SiMCM-41 was incorporated into Al_2O_3 and Al_2O_3–TiO_2. Catalytic activity was established in terms of DBT conversion. The catalysts were characterized by S_{BET}, TPD-NH_3, TPR, SEM and XPS techniques.

2. Experimental

A binary oxide Al_2O_3–TiO_2 containing 20 wt.% of TiO_2 was prepared by deposition of TiO_2 on the surface of aluminium hydroxide (PURAL KR1, Sasol GmbH; boehmite, S_{BET} = 304 m^2/g). According to the preparation procedure, isopropyl alcohol solution of titanium(IV) isopropoxide was added to aluminium hydroxide suspended in isopropanol alcohol. To obtain a molar ratio of H_2O:TIPOT = 4:1, ammonium water was added during continuous mixing of the solution. The sol was gelated at room temperature for 15 h. The samples were placed and dried up at stepwise increased temperature: at 30, 50, 70 and 90 °C for 0.5 h; at 110 °C for 12 h.

The SiMCM-41 (referred to as MCM-41) was synthesized using tetraethyl orthosilicate (TEOS), tetramethylammonium hydroxide (TMAOH) and cetyltrimethylammonium bromide (CTMABr) as template according to the synthesis procedure described elsewhere [9].

The calcined MCM-41 was mixed with alumina hydrogel or alumina–titania hydrogel, peptized with 3% nitric acid and then extruded. The extruded supports were dried at room temperature for 24 h and at 110 °C for 12 h and thereafter calcined at 500 °C for 3 h. The conventional two-step impregnation of the extrudates was performed with a water solution of $(NH_4)_6Mo_7O_{24}{\cdot}4H_2O$ (14 wt.% of MoO_3) and $Ni(NO_3)_2{\cdot}6H_2O$ (3 wt.% of NiO). The thermal treatment of the molybdenum and nickel–molybdenum catalysts was carried out under the same conditions as for the extruded supports.

Nitrogen adsorption was measured at 77 K, using a Quantachrome Autosorb Automated Gas Sorption Analyzer. Prior to adsorption measurements, the sample was outgased under vacuum at 250 °C for 1 h. The specific surface area was calculated using the standard BET method. The pore size distribution was determined using the Barrett–Joyner–Hatenda (BJH) algorithm and DFT-Monte Carlo method. Macropore size distribution was measured by mercury porosimetry (Carlo Erba, Pascal 440).

Molybdenum and nickel content was determined by inductively coupled plasma-atomic emission spectroscopy. Measurements were performed on a Varian model VISTA-MPX, CDD Simultaneous Apparatus. The two-step (HNO_3, HCl) demineralization procedure was carried out in a microwave oven (MARS 5, CEM).

The acidity of the catalysts was determined by temperature-programmed desorption of ammonia (TPD-NH_3). The samples were pre-treated in a stream of argon at 550 °C for 2 h and afterwards cooled to 180 °C. After desorption of physically adsorbed ammonia (at 180 °C) the samples were heated at a rate of 10 °/min in a stream of argon up to 550 °C. Desorbed ammonia was detected by the GC method.

The temperature-programmed reduction (TPR) of the catalysts was performed in an ALTAMIRA automated system (AMI-1), with an Ar/H_2 mixture (95/5 v/v, 20 cm^3/min) at a heating rate of 10 °/min. After reaching 800 °C, the samples were kept in this environment for 1 h and finally the catalysts were cooled in a stream of argon. The TPR-TPO experiments involved the following cycles:

TPR up to 800 °C (TPR I)
→ TPO 500 °C → TPR up to 800 °C (TPR II).

Hydrogen uptake was calibrated with reference to the TPR peak of known amounts of the standard (pure NiO).

XPS measurements were performed using a SPECS PHOIBOS 100 hemispherical analyzer equipped with a magnesium source (1253.6 eV) operating at 100 W (wide-range scan) and 200 W (high-resolution spectra). The spectrometer energy scale was calibrated using Au $4f_{7/2}$, Ag $3d_{5/2}$ and Cu $2p_{3/2}$ lines at 84.2, 367.9 and 932.4 eV, respectively. The analyzer mode was set at constant pass energy of 30 eV in survey, and 5 eV in narrow scans. The detection angle was normal to the sample surface. The base pressure in the UHV analysis chamber was lower than 5×10^{-10} mbar. Energy shift due to the static charging of the samples was corrected with the C 1s peak at 284.6 eV as a reference. The spectra were collected and processed using SpecsLab software. The accuracy of the reported binding energies was ±0.1 eV. Element concentrations were evaluated from peak areas after Shirley background subtraction.

Scanning electron microscopy (SEM) observations were carried out using a Jeol JSM 5888 LV electron microscope equipped with an Oxford Isis system for microanalysis. Prior to analysis, the samples were sprayed with an approximately 100 nm thick carbon layer. The molybdenum distribution for Mo Kα lines was determined.

HDS of DBT in decaline (0.35 wt.% S) was performed in a high-pressure fixed-bed microreactor. Catalytic activity was evaluated at 345 °C (p, 6.0 MPa; LHSV, 3.0 h^{-1}; H_2:CH, 350 Nm^3/m^3). The catalysts were sulphided in situ using a solution of diethyl sulphide in decaline (1.5 wt.% S), until H_2S in the outlet gas was detected, and then continued for 1 h. Sulphur concentrations in the feed and products were analyzed by XRD fluorescence spectroscopy (Phillips PW 1400). DBT HDS products were identified by GC–MS and GC-FID equipped with an RTX-1 capillary column (100% dimethyl polysiloxane, 60 m, 0.53 mm, 1.0 μm).

3. Results and discussion

Chemical composition, textural parameters and acidity of the investigated catalysts are shown in Table 1.

Examinations of the metal (metals) content in the catalysts have produced the following finding: despite the same assumed amount of MoO_3 (14 wt.%) incorporated by impregnation, the

Table 1
Textural parameters and acidity related to the chemical composition of the catalysts

Catalyst code	Support composition	MoO_3 (wt.%)	NiO (wt.%)	Acidity (mmol NH_3/g)	S_{BET} (m^2/g)	TV_p[a] (cm^3/g)	V[b] (cm^3/g)	V[c] (cm^3/g)	S[d] (m^2/g)	S[e] (m^2/g)	V[f] (cm^3/g)
KM-1	Al_2O_3	13.5	2.5	0.508	230.4	0.54	0.53	0	325.74	0	0.50
KM-12	Al_2O_3	13.5	–	–	–	–					
KM-7	Al_2O_3–TiO_2	12.8	2.4	0.433	227.9	0.57	0.50	0	301.64	0	0.49
KM-13	Al_2O_3–TiO_2	12.8	–	–	–	–					
KM-3	Al_2O_3:MCM-41 = 1:1	10.8	2.4	0.249	540.1	0.49	0.23	0.24	162.05	319.00	0.47
KM-14	Al_2O_3:MCM-41 = 1:1	10.8	–	–	–	–					
KM-9	Al_2O_3–TiO_2:MCM-41 = 1:1	11.9	2.5	0.197	540.9	0.51	0.25	0.21	157.96	292.08	0.47
KM-15	Al_2O_3–TiO_2:MCM-41 = 1:1	11.9	–	–	–	–					
KM-11	MCM-41	10.7	2.6	0.117	666.3	0.45	0.08	0.31	36.06	461.03	0.39
KM-16	MCM-41	10.7	–	–	–	–					

[a] Total pore volume calculated at adsorption–desorption point.
[b] Pore volume in the pore diameter range of 4–50 nm estimated by BJH method.
[c] Pore volume in the pore diameter range of 0–4 nm estimated by DFT method.
[d] Surface area of pore in the pore diameter range of 4–50 nm estimated by BJH method.
[e] Surface area of pore in the pore diameter range of 0–4 nm estimated by DFT method.
[f] Mesopore volume.

content of MoO_3 in MCM-41 containing catalysts was by about 3 wt.% lower than that in the Al_2O_3 or Al_2O_3–TiO_2 catalyst. This may, one hand, be due to the weaker interaction between silica and ammonium heptamolybdate than between alumina and ammonium heptamolybdate (a higher PZC for alumina than silica), as well as, on the other hand, the partial blocking of the MCM-41 channels by ammonium heptamolybdate. Irrespective of the composition of the support, the content of NiO (also incorporated by impregnation, assumed for 3 wt.% of NiO) was comparable in all the catalysts tested, amounting to about 2.5 wt.%. One can expect that the differences between PZC for Mo/alumina and Mo/silica are smaller, than the differences between alumina and silica, therefore amounts of adsorbed nickel nitrate are comparable.

The textural parameters (Table 1) of the investigated catalysts show that the two-fold increase in the specific surface area should be attributed to the incorporation of MCM-41 into Al_2O_3 and Al_2O_3–TiO_2 supports. As for the pore size distribution, there is no difference between the catalyst NiMo/Al_2O_3 (KM-1) and the catalyst NiMo/Al_2O_3–TiO_2 (KM-7) in the range of 1.5–50 nm (Fig. 1b). For these catalysts sharp peaks are centred around 5 nm. The pore size distribution in the macropore range (above 50 nm) shows that TiO_2 deposition onto the Al_2O_3 surface increases the proportion of macropores. It should be noted that, compared to the KM-1 catalyst, the maximum pore volume for KM-7 is shifted towards larger pore diameters (from 475 nm for KM-1 to 1120 nm for KM-7). With catalysts which contain MCM-41, as a mesopore-forming component, textural modification is observed in the range of both mesopores and macropores. NiMo/Al_2O_3-MCM-41 (KM-3) and NiMo/Al_2O_3–TiO_2-MCM-41 (KM-9) display similar mesopore volume distributions in the range of 2–4 nm; compared to the NiMo/MCM-41 (KM-11) catalyst, the maxima are shifted towards larger pore diameters. Since the proportion of macropores in the catalyst containing MCM-41 alone (10 wt.% of alumina binder) is small, its incorporation into Al_2O_3 or Al_2O_3–TiO_2 noticeably reduces the proportion of macropores in the Al_2O_3-based, especially in the Al_2O_3–TiO_2-based catalysts (though the proportion of macropores in KM-9 is still the highest) (Fig. 1a).

The results of TPD-NH_3 for NiMo catalysts showed that the incorporation of MCM-41 into alumina and alumina–titania supports has decreased the acidity of the catalysts (Table 1). Total acidity of the MCM-41 containing catalysts (KM-3, KM-9) was about two-fold lower than that of the NiMo/Al_2O_3 (KM-1) and NiMo/Al_2O_3–TiO_2 (KM-7) catalysts. However, the incorporation of TiO_2 into Al_2O_3 also accounts for the decrease in acidity. The TPD-NH_3 profiles (Fig. 2) of all NiMo catalysts are rather similar in shape (consisting of one broad peak with maximum between 300 and 350 °C) but differ in the amount of ammonia desorbed and in the acid site distribution. With the MCM-41-based NiMo catalyst, most of the ammonia is desorbed in the range of 270–350 °C as compared to catalysts supported on Al_2O_3 and Al_2O_3–TiO_2. The drop in acidity and the changes in acid site distribution are due to the 'dilution' of Al_2O_3 and Al_2O_3–TiO_2 by MCM-41, which contains mainly such acid sites where ammonia is desorbed below 350 °C.

The TPR results for Mo catalysts are shown in Fig. 3. The TPR profiles of the catalysts reflect distinctly the difference in reducibility between KM-16 (Mo/MCM-41) and both KM-14 (Al_2O_3-MCM-41) and KM-15 (Mo/Al_2O_3–TiO_2-MCM-41). The TPR profile of KM-16 exhibits one broad TPR peak with maximum centred at 595 °C. The TPR pattern of KM-14 and that of KM-15 have many features in common and display two low-temperature peaks: one at about 470 °C and the other one at about 540 °C. This finding suggests that the interactions between Mo species and the mixed supports are weaker than those between Mo species and MCM-41. According to literature data [10] and our XPS results (Fig. 4), the two peaks observed in the TPR profile between 400 and 600 °C correspond with the first step of reduction of polymeric octahedral coordinated molybdenum oxo-species ($Mo^{+6} \rightarrow Mo^{+4}$), which differ in reducibility. Similar reducibility has been observed for Mo oxo-species supported on amorphous silica–alumina [11]. The results prove that MCM-41 influences

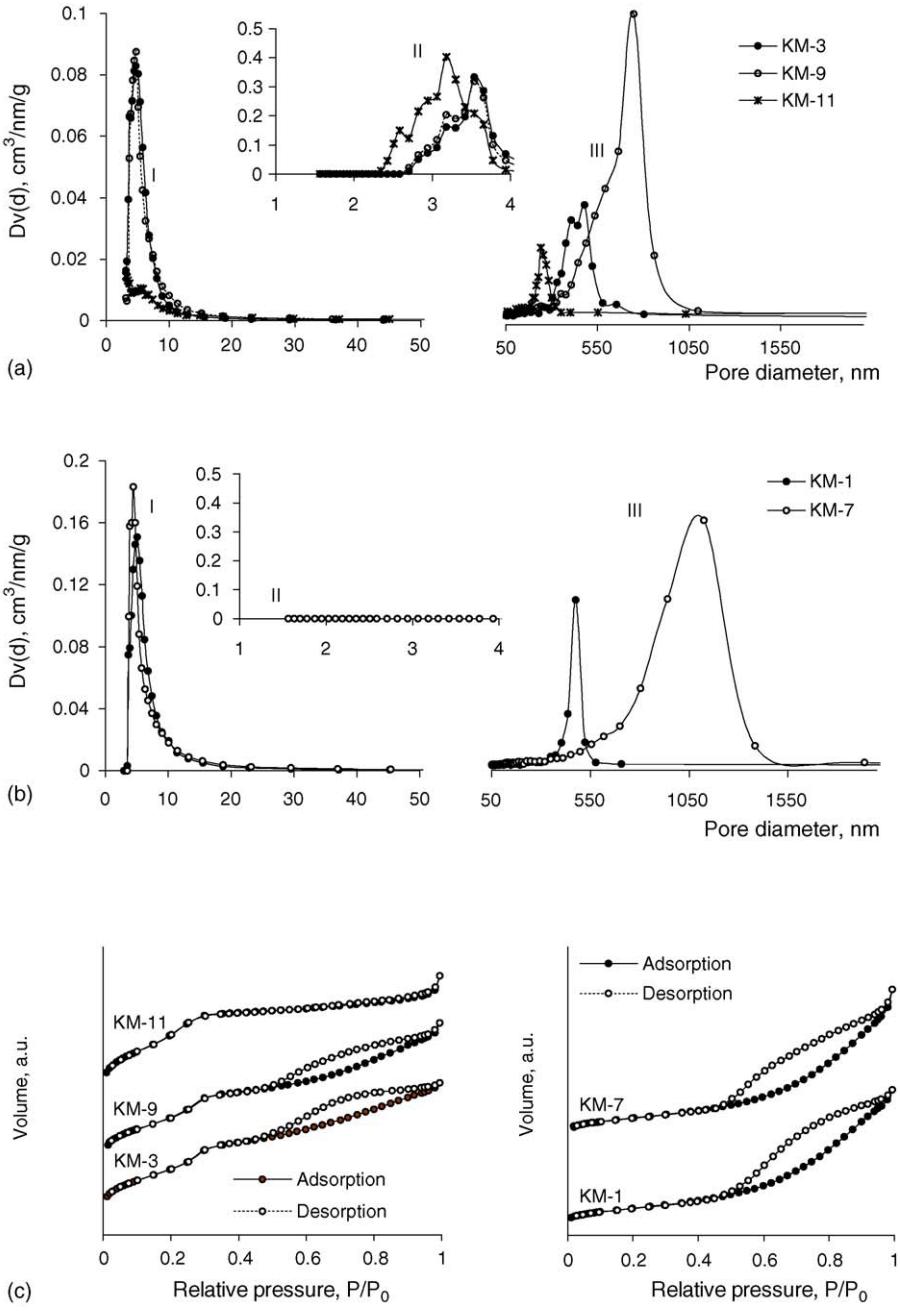

Fig. 1. Pore volume distribution of NiMo catalysts; (I) pore size distribution, BJH method; (II) pore size distribution, DFT-Monte Carlo method; (III) pore size distribution, mercury porosimetry ((a) and (b)); nitrogen adsorption–desorption isotherms (c).

also the high-temperature reduction region (above 600 °C). This means that the presence of mesoporous MCM-41 accounts for the decrease in the amount of Mo oxo-species, which are the most difficult to reduce. According to some investigators [10,12,13], the reduction region above 600 °C can be linked with the second step of the reduction of octahedral polymeric molybdenum species ($Mo^{+4} \rightarrow Mo^{0}$), as well as of tetrahedral monomeric molybdenum species ($Mo^{+6} \rightarrow Mo^{0}$). It is worth noticing that in the presence of MCM-41 the promoting effect of TiO_2 on the reducibility of Mo species decreases remarkably (compare KM-12 to KM-13 and KM-15).

The comparison of the TPR I profiles for Mo/MCM-41 (KM-16; Fig. 3) and NiMo/MCM-41 (KM-11; Fig. 5) has revealed a strong promoting effect of nickel on the reducibility of MoO_3. The maximum of the main peak at 595 °C for KM-16 (reduction of Mo oxo-species) is shifted by ca. 120 °C towards lower temperatures for KM-11. As for KM-11, the maximum of the main peak at 472 °C is associated with the reduction of both Mo oxo-species and NiO oxo-species (overlapping of MoO_3 and NiO reduction regions). The TPR II profiles for KM-11 (Fig. 5) following reoxidation of the catalyst at 500 °C shows a peak at much higher temperature (595 °C) and is similar to the TPR I profile of KM-16. The occurrence of the maximum at 595 °C for KM-11 in TPR II can be attributed to a stronger interaction of the nickel phase with the support and/or to the penetration of the nickel phase into the support interior (most

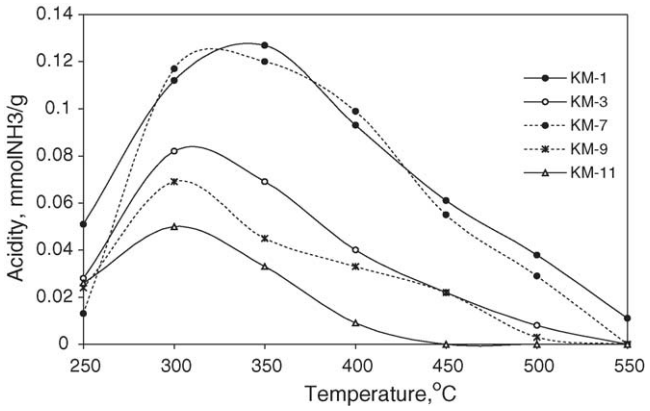

Fig. 2. TPD-NH_3 patterns for NiMo catalysts.

probably due to the thermal processing continued up to 800 °C during the TPR I run).

It should be noted that it is not only temperature but also time that affects reducibility. The effect of time on the reducibility of MoO_3 has been reported elsewhere [14,15]. Thus, following the reduction of MoO_3 at atmospheric pressure and at 500 °C for 3 h, approximately 75% of the total molybdenum was present as Mo^{+4} [14]. Under the conditions mentioned above, Mo^{+6} is reduced completely to Mo^{+4} after 12 h [15].

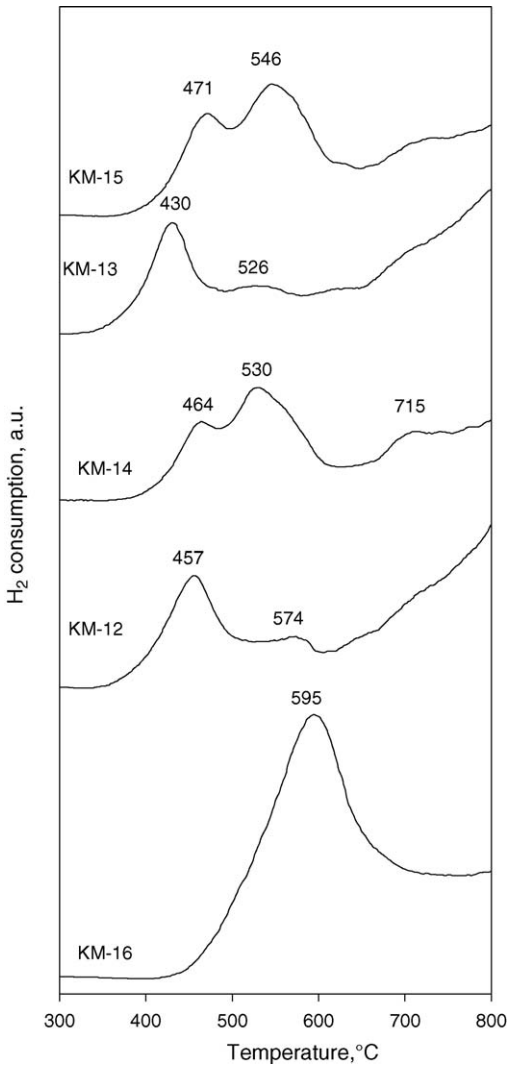

Fig. 3. TPR I profiles for Mo catalysts.

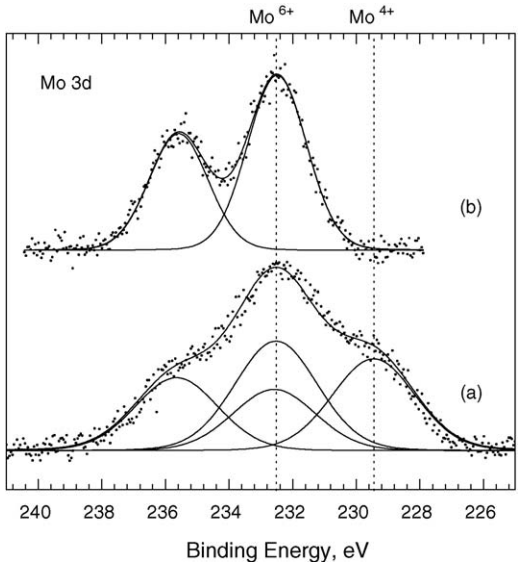

Fig. 4. XPS spectra of Mo 3d region of Mo oxo-species for KM-14: (a) before reduction; (b) after reduction (6 MPa; 470 °C; 3 h).

In our study, consideration was also given to the problem of how preliminary high-pressure treatment with H_2 of NiMo/MCM-41 catalyst influences the reducibility of that catalyst during TPR I run. The result for the catalyst referred to as KM-11R – after hydrogen treatment (at 6 MPa and 470 °C for 3 h, at a flow rate of 70 cm^3/min), followed by reoxidation (in air flow under the same conditions as those used for catalyst

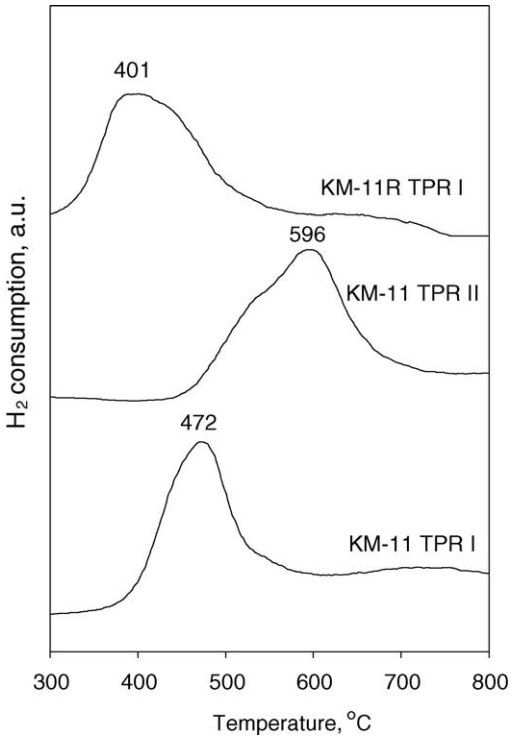

Fig. 5. TPR profiles for NiMo catalysts.

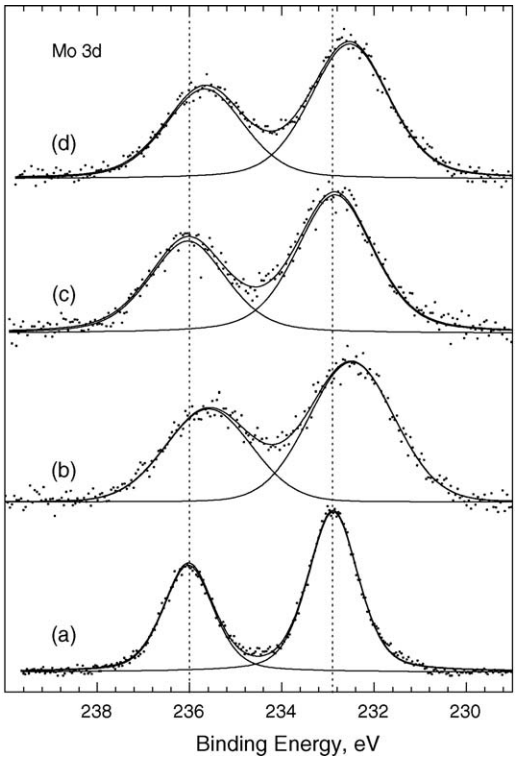

Fig. 6. XPS spectra of Mo 3d region of: MoO_3 (a); KM-14 (b); KM-15 (c); KM-16 (d).

preparation; 500 °C; 3 h) – is presented in Fig. 5 (KM-11R TPR I). The TPR I profile shows a maximum hydrogen uptake at a temperature by 70 °C lower than that for the non-treated catalyst (KM-11) (T_{MAX} at 400 and 470 °C, respectively). The results imply that the catalyst treatment under hydrogen pressure at 6 MPa influences the reducibility of the metal oxo-species. The reduction of NiMo/MCM-41 under hydrogen pressure leads to the formation of polymeric octahedral molybdenum species weakly bounded to the support.

Table 2
XPS data for molybdenum catalysts

	Mo $3d_{5/2}$	Mo $3d_{3/2}$	FWHM
KM-14	232.49	235.60	2.25
KM-15	232.83	236.07	2.01
KM-16	232.52	235.70	2.05
MoO_3	232.90	236.02	1.30

Fig. 6 shows the Mo 3d spectra for pure MoO_3 and MCM-41 containing molybdenum catalysts. The Mo $3d_{5/2}$–Mo $3d_{3/2}$ doublet was fitted so that each peak had the same Gaussian line shape and width (FWHM). The MoO_3 was obtained by calcination of ammonium heptamolybdate ($(NH_4)_7Mo_7O_{24}{\cdot}4H_2O$) at 550 °C for 6 h.

The spectrum for the as prepared MoO_3 in the Mo 3d region showed the presence of two well-resolved spectral lines at 232.90 and 236.02 eV (FHWM = 1.3). This binding energy (BE) was assigned to the Mo $3d_{5/2}$ and Mo $3d_{3/2}$ spin–orbit components, respectively. The BE of the Mo $3d_{5/2}$ and Mo $3d_{3/2}$ of Mo/Al_2O_3-MCM-41 (KM-14) and Mo/MCM-41 (KM-16) shifts to lower energies by about 0.4 eV as compared with those of bulk MoO_3 (Table 2). According to some investigators [16,17], the broadening in FWHM can be regarded as evidence that MoO_3 has better dispersed on

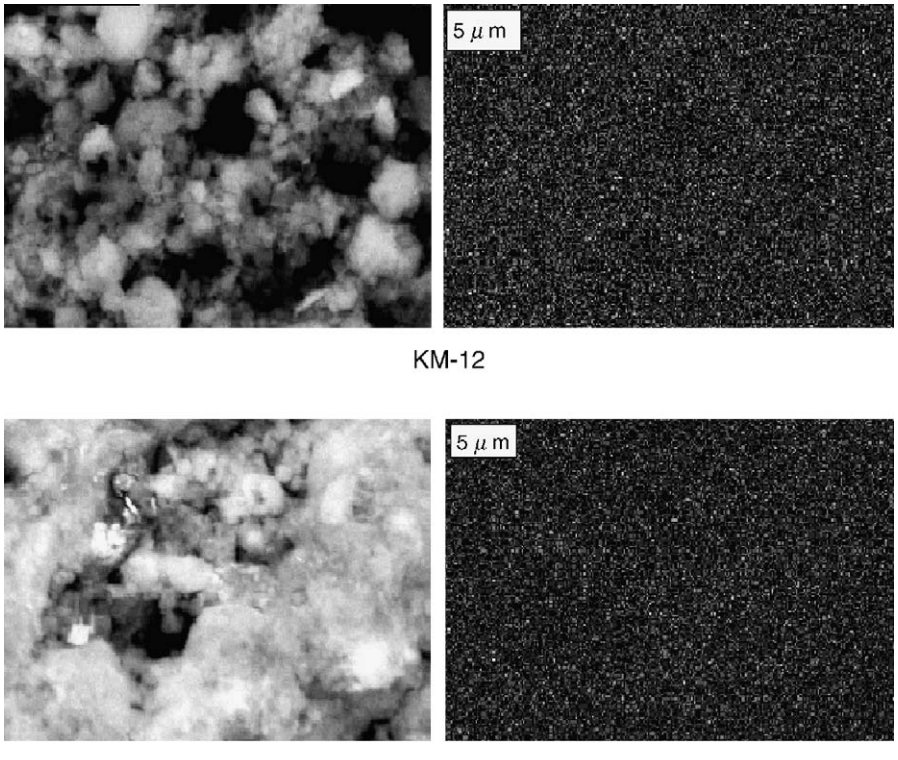

Fig. 7. SEM micrographs of molybdenum catalysts supported on Al_2O_3 and Al_2O_3–TiO_2.

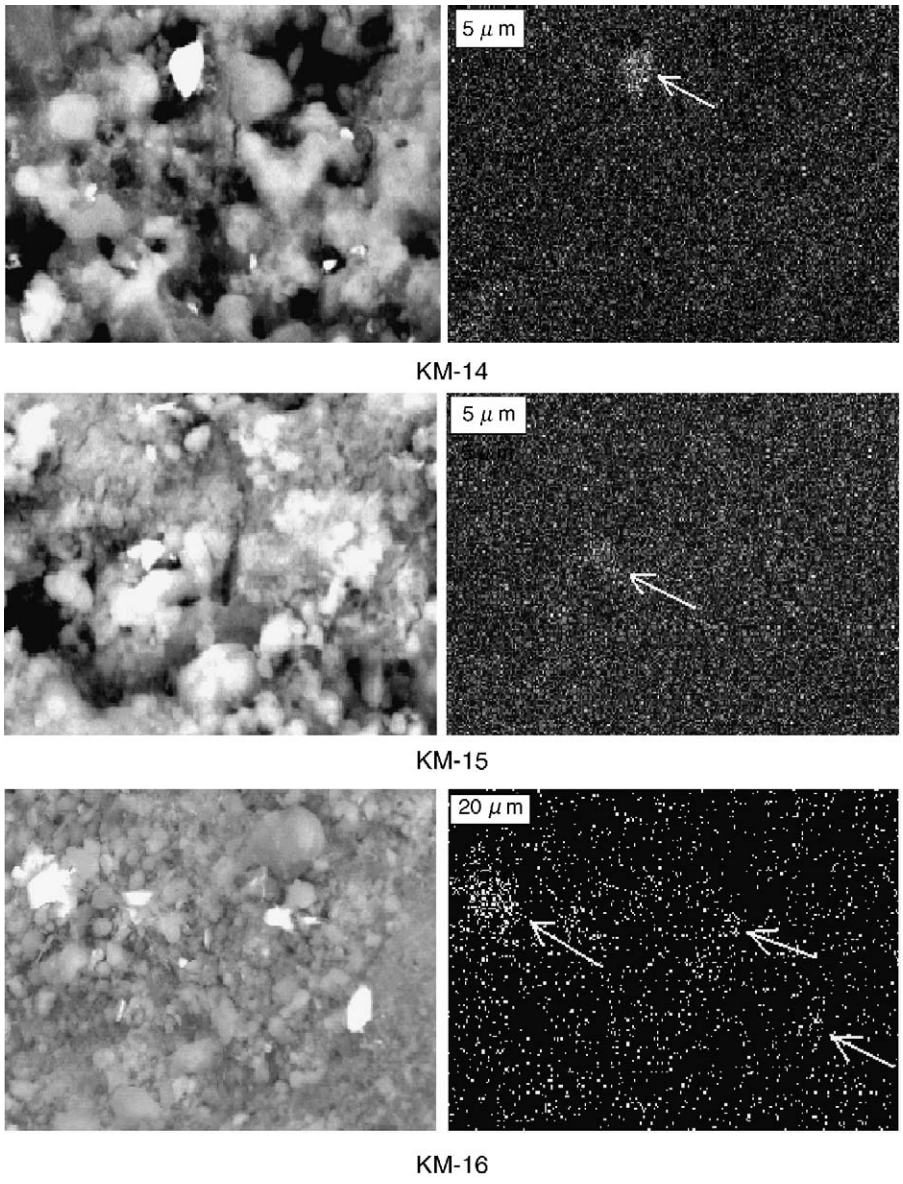

Fig. 8. SEM micrographs of molybdenum catalysts containing MCM-41.

the Al_2O_3-MCM-41 support (KM-14) than on the MCM-41 support (KM-16). The BE of the Mo $3d_{5/2}$ and Mo $3d_{3/2}$ for Mo/Al_2O_3–TiO_2-MCM-41 (KM-15) amounts to 232.83 and 236.07 eV, respectively. It is higher than the BE of KM-14 and KM-16. The higher BE for KM-15 is convincing evidence of a stronger molybdenum-support interaction as compared to the KM-14 and KM-16 catalysts. The stronger interaction between the Mo species and Al_2O_3–TiO_2-MCM-41 support than between the Mo species and Al_2O_3-MCM-41 support was also confirmed by TPR (Fig. 3).

As shown by Figs. 7 and 8, Mo/Al_2O_3 (KM-12) and Mo/Al_2O_3–TiO_2 (KM-13) displayed a homogeneous dispersion of molybdenum in contrast to the catalyst containing MCM-41 (KM-14 and KM-15). Microelemental analysis revealed that the presence of MCM-41 influenced not only the Mo agglomeration on the catalyst surface, but also the Mo distribution along the cross-section of the extrudates (Fig. 9).

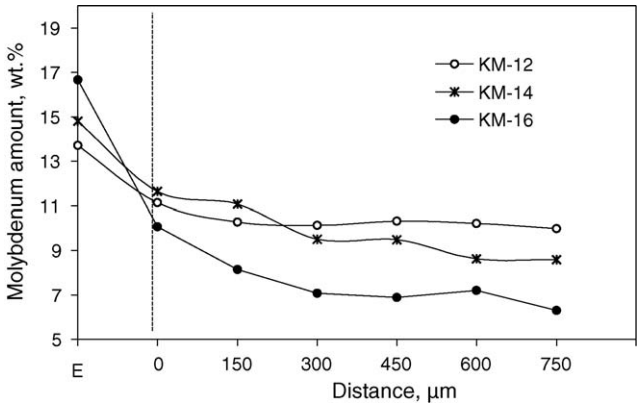

Fig. 9. Molybdenum distribution along the cross-section of the extrudates: E, external surface; 0 μm, edge of the extrudates; 750 μm, centre of the extrudates.

Table 3
Results of DBT HDS over Mo and NiMo catalysts

	NiMo catalysts				
	KM-1 (support Al_2O_3)	KM-3 (support Al_2O_3 -MCM-41)	KM-11 (support MCM-41)	KM-9 (support Al_2O_3 –TiO_2-MCM-41)	KM-7 (support Al_2O_3 –TiO_2)
DBT conversion (%)	85.2	80.5	81.7	88.1	92.6
Product distribution (wt.%)					
BCH	14.3	–	–	–	6.5
CHB	51.0	3.8	4.4	3.9	44.1
BP	34.7	96.2	95.6	96.1	49.4
	Mo catalysts				
	KM-12 (support Al_2O_3)	KM-14 (support Al_2O_3 -MCM-41)	KM-16 (support MCM-41)	KM-15 (support Al_2O_3 –TiO_2-MCM-41)	KM-13 (support Al_2O_3 –TiO_2)
DBT conversion (%)	64.9	69.5	66.1	71.2	86.1

The amount of Mo was measured on the external surface and every 150 μm from the edge to the centre of the extrudates. It should be noted that the incorporation of MCM-41 into the alumina support (KM-14) increased Mo concentration on the external surface and decreased on successive layers above 300 μm. As for the catalyst on MCM-41 as a support (KM-16), the differences between Mo concentration along the cross-section of the extrudates were the greatest. The inhomogeneity of Mo dispersion and the increase of Mo concentration on the external surface of KM-16 can be explained by partial blocking of the MCM-41 channels by ammonium heptamolybdate during the impregnation procedure. These results are in line with the behaviour of AlMCM-41 containing catalysts [7].

Table 3 shows DBT HDS conversion evaluated at 345 °C. The results of DBT conversion show that Mo and NiMo catalysts supported on Al_2O_3–TiO_2 possess higher activity than those supported on Al_2O_3. The promoting effect of nickel on the activity of molybdenum catalysts is more pronounced in the case of Al_2O_3. It was found that when MCM-41 was incorporated into the supports, the nickel loading favoured the DBT HDS reaction to a greater extent when Al_2O_3–TiO_2 was used for catalyst preparation (compare KM-9 and KM-3). The modification of the Al_2O_3–TiO_2-MCM-41-supported molybdenum catalyst by incorporating nickel brings about a greater rise in catalytic activity (DBT conversion) than when nickel is incorporated into the molybdenum catalyst with no MCM-41 in the Al_2O_3–TiO_2 support.

According to literature data [18–20], the transformation of DBT occurs through two parallel reactions: (i) direct desulfurization (DDS) yielding biphenyl (BP), and being a measure of DBT hydrogenolysis, and (ii) desulfurization after hydrogenation (HYD), yielding tetrahydrodibenzothiophene (THDBT) and then cyclohexylbenzene (CHB) and bicyclohexyl (BCH). The DBT HDS products are BP, CHB, BCH, and traces of THDBT. The results show that the BP/(CHB + DCH) ratio is higher for catalysts containing MCM-41 than for NiMo/Al_2O_3 and NiMo/Al_2O_3–TiO_2 catalysts. Therefore, we conclude that over catalysts containing MCM-41 the desulphurization of DBT runs mostly via the DDS route. According to literature data [21], the rate of BP hydrogenation is remarkably low in the presence of DBT, because DBT successfully competes with BP for the hydrogenation over active sites.

In contrast to the results reported elsewhere [22], we found that the DBT HDS by the DDS route is more favourable for the NiMo/Al_2O_3–TiO_2 than NiMo/Al_2O_3 catalyst.

4. Conclusions

On the basis of the results obtained the following conclusions can be drawn:

1. The incorporation of MCM-41 into Al_2O_3 or Al_2O_3–TiO_2 disturbs the homogeneity of MoO_3 dispersion on the external surface of the catalysts;
2. The presence of MCM-41 in the support retards the promoting effect of TiO_2 on the reducibility of molybdenum oxide;
3. The NiMo catalyst supported on MCM-41 alone, or having a support with MCM-41 as one of the components, is less efficient in DBT HDS than the catalysts supported on Al_2O_3 or Al_2O_3–TiO_2;
4. From the distribution of DBT HDS products we can conclude that over catalysts containing MCM-41 the desulphurization of DBT runs mostly via the DDS route.

Acknowledgement

This work was supported by the National Committee for Scientific Research of the Ministry of Science Research and Informatization, Poland (Grants 4 T09B 080 22 and 3 T09B 112 26).

References

[1] D.D. Whitehurst, H. Farag, T. Nagamatsu, K. Sakanishi, I. Mochida, Catal. Today 45 (1998) 299.

[2] N. Kunisada, K.H. Choi, Y. Korai, I. Mochida, K. Nakano, Appl. Catal. A: Gen. 279 (2005) 253.
[3] U. Nylen, J.F. Delgado, S. Järås, M. Boutonnet, Fuel Proc. Technol. 86 (2004) 223.
[4] K.Y.S. Ng, E. Gulari, J. Catal. 95 (1985) 33.
[5] M. Breysse, P. Afanasiev, Ch. Geantet, M. Vrinat, Catal. Today 86 (2003) 5.
[6] K.M. Reddy, B. Wei, C. Song, Catal. Today 43 (1998) 261.
[7] M. Cheng, F. Kumata, T. Saito, T. Komatsu, T. Yashima, Appl. Catal. A: Gen. 183 (1999) 199.
[8] Ramírez, R. Contreras, P. Castillo, T. Klimova, R. Zárate, R. Luna, Appl. Catal. A: Gen. 197 (2000) 69.
[9] W.A. Carvalho, P.B. Varaldo, M. Wallau, U. Schuchardt, Zeolites 18 (1997) 408.
[10] Yu.V. Plyuto, I.V. Babich, I.V. Plyuto, A.d. Van Langeveld, J.A. Moulijn, Colloids Surf. A: Physicochem. Eng. Aspects 125 (1997) 225.
[11] L. Qu, W. Zhang, P.J. Kooyman, R. Prins, J. Catal. 215 (2003) 7.
[12] T. Klimova, L. Lizama, J.C. Amezcua, P. Roquero, E. Terres, J. Navarrete, J.M. Dominguez, Catal. Today 98 (2004) 141.
[13] T. Chiranjeevi, P. Kumar, M.S. Rana, G. Murali Dhar, T.S.R. Prasada Rao, J. Mol. Catal. 181 (2002) 109.
[14] J.G. Choi, L.T. Thompson, Appl. Surf. Sci. 93 (1996) 143.
[15] D.S. Zing, L.E. Makovsky, R.E. Tischer, F.R. Brown, D.M. Hercules, J. Phys. Chem. 84 (1980) 2898.
[16] Z. Li, L. Gao, S. Zheng, Appl. Catal. A: Gen. 236 (2002) 163.
[17] Z. Li, L. Gao, S. Zheng, Mater. Lett. 57 (2003) 4605.
[18] J.J. Lee, H. Kim, S.H. Moon, Appl. Catal. B: Environ. 41 (2003) 171.
[19] P. Michaud, J.L. Lemberton, G. Pérot, Appl. Catal. A: Gen. 169 (1998) 343.
[20] A. Wang, Y. Wang, T. Kabe, Y. Chen, A. Ishihara, W. Qian, J. Catal. 199 (2001) 19.
[21] H. Farag, D.D. Whitehurst, K. Sakanishi, I. Mochida, Catal. Today 50 (1999) 49.
[22] S. Yoshinaka, K. Segawa, Catal. Today 45 (1998) 293.